Experimental demonstration of an electrostatic orbital angular momentum sorter for electron beams: Supplementary Material

Amir H. Tavabi[1], Paolo Rosi[2], Enzo Rotunno[3], Alberto Roncaglia[4], Luca Belsito[4], Stefano Frabboni[2,3], Giulio Pozzi[1,5], Gian Carlo Gazzadi[3], Peng-Han Lu[1,6], Robert Nijland[7], Moumita Ghosh[7], Peter Tiemeijer[7], Ebrahim Karimi[8], Rafal E. Dunin-Borkowski [1], Vincenzo Grillo[3]

1. Ernst Ruska-Centre for Microscopy and Spectroscopy with Electrons and Peter Grünberg Institute, Forschungszentrum Jülich, 52425 Jülich, Germany
2. Dipartimento FIM, Universitá di Modena e Reggio Emilia, 41125 Modena, Italy
3. Centro S3, Istituto di nanoscienze-CNR, 41125 Modena, Italy
4. Istituto per la Microelettronica e i Microsistemi-CNR, 40129 Bologna, Italy
5. Department of Physics and Astronomy, University of Bologna, 40127 Bologna, Italy
6. RWTH Aachen University, 52074 Aachen, Germany
7. Thermo Fisher Scientific, PO Box 80066, 5600 KA Eindhoven, The Netherlands
8. Department of Physics, University of Ottawa, Ottawa, Ontario K1N 6N5, Canada

A1: Complex notation expanded

According to the main text, the phase distributions introduced by the sorters are

$$\varphi_1 = \frac{s}{\lambda}\,\Re e\left\{\mathrm{u}\ln\left(\frac{u}{L}\right) - u\right\}\,, \tag{A1}$$

$$\varphi_2 = \frac{Ls}{\lambda}\,\Re e\left\{\exp\left(\frac{u}{sf}\right)\right\}\,. \tag{A2}$$

Expansion of the complex notation for sorter 1 in the form

$$\varphi_1 = \frac{s}{\lambda}\,\Re e\left\{(\mathrm{x}+\mathrm{iy})\left[ln\left(\frac{\sqrt{x^2+y^2}}{L}\right) + i\mathrm{atan}\,(y,x)\right] - (x+iy)\right\}$$

leads to the expression

$$\varphi_1 = \frac{s}{\lambda}\left\{x\,ln\left(\frac{\sqrt{x^2+y^2}}{L}\right) - y\,\mathrm{atan}(y,x) - x\right\}\,.$$

For sorter 2,

$$\varphi_2 = \frac{Ls}{\lambda}\left\{\exp\left(\frac{x}{sf}\right)cos\left(\frac{y}{sf}\right)\right\}\,. \tag{A3}$$

These are the equations that are conventionally used to describe an OAM sorter. Their gradients can be defined in the form of Wirtinger derivatives $\frac{\partial\varphi_1}{\partial\bar{u}} := (\frac{\partial}{\partial x} + i\frac{\partial}{\partial y})$ as

—— – (A4)

—— — .

A2: Holograms and generated beams

We reported scanning electron microscopy (SEM) images of some of the "generator" holograms. The first example corresponds to an inline vortex, which is characterized by the thickness function

, (A5)

where "mod" refers to a remainder following division of the two arguments. The OAM spectrum of such a mask has been calculated in Ref. [27].

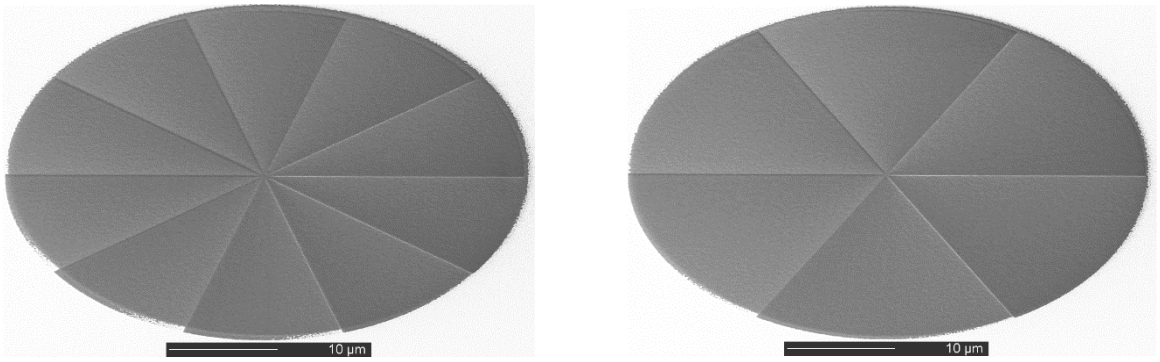

Fig A1: Tilted SEM images of holograms with angular frequencies corresponding to ℓ = 10 and ℓ = 6.

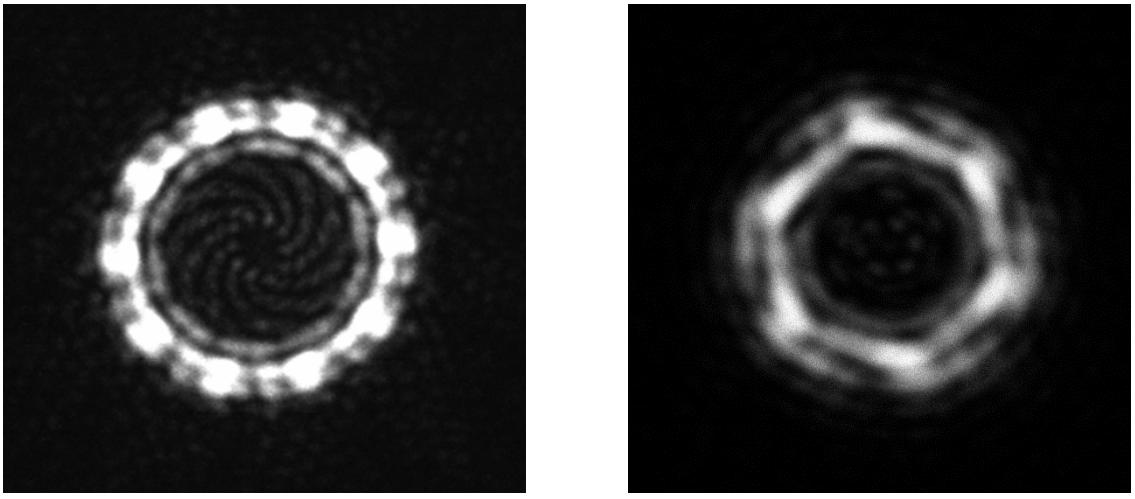

Fig A2: Beams corresponding to the holograms in Fig. A1. 10-fold and 6-fold modulations in intensity result from the presence of a strong ℓ=0 component, which is visible in experimental OAM spectra.

The second mask is based on a thickness modulation of the form

$$\mathrm{T} = \begin{cases} t_0 & if\ 0 < \mathrm{mod}(n\theta, 2\pi) < \pi \\ t_0 + t_1 & if\ \pi < \mathrm{mod}(n\theta, 2\pi) < 2\pi \end{cases} \quad \text{(A6)}$$

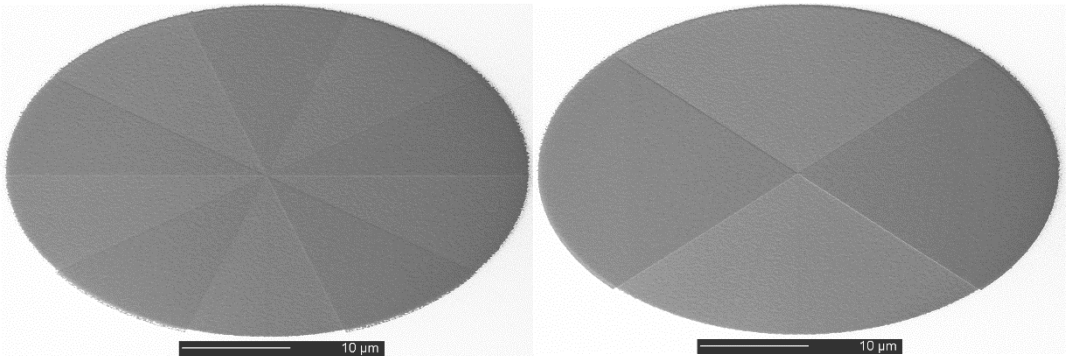

Fig A3:Tilted SEM images of holograms for the generation of petal beams for ℓ = ±5 (left) and ℓ = ±2 (right).

A3: Validation of OAM decomposition

In this section, OAM decomposition is validated by using direct images of the electron beam in real space with the probe close to its waist.

Normally, determination of the OAM decomposition of a beam from a real space image is impossible because the phase of the beam is lost during the measurement. However, in the case of a petal beam, which is given by a superposition of beams of vortices with opposite OAM $\ell = \pm n,$ one can simplify the calculation since the beam wavefunction only has a real component. By expressing a vortex in the form $\psi = R_{|\ell|}(\rho)\exp\,(i\,\ell\theta)$, where $R_{|\ell|}(\rho)$ is a radial function, the corresponding petal beam takes the form $\psi = R_{|\ell|}(\rho)\sin\,(\ell\theta)$.

The inline hologram that we used to generate petal beams is described by Eq. A6. For this specific hologram, the angular and radial degrees of freedom are decoupled and the azimuthal part of the wavefunction can be factorized in the form

$$\Theta(\theta) = \sum_{\ell} c_\ell \exp(i\,\ell\theta)\ .$$

The coefficients of OAM expansion for a perfect phase hologram are

$$c_\ell = \begin{cases} \frac{-2ni}{\ell\pi}\exp(i\delta/2)\sin\left(\frac{\delta}{2}\right) & if\quad \ell = mn \\ \exp(i\delta/2)\cos\left(\frac{\delta}{2}\right) & if\quad \ell = 0 \\ 0 & otherwise\ , \end{cases} \quad \text{(A7)}$$

where δ is the phase corresponding to a depth t_1 of milling and *m* is an odd integer.

To a first approximation, the series can be limited to only the first terms, for which $\ell = \pm n$ and $\ell = 0$. The wavefunction is then given by the expression

$$\psi = 2\,|c_n|\sin(n\theta) + \mathrm{i}|c_0| \ . \qquad \text{(A8)}$$

This expression differs from that of an exact petal beam because of the presence of the c_0 term, which arises if the hologram depth is not perfectly calibrated to have $\delta = \pi$. In practice, it can be difficult to make this calibration precisely.

The absolute value was used here to highlight the fact that for a perfect phase hologram the 0^{th} order and the first nonzero diffractions have exactly a π/2 phase difference.

The resulting image can be expressed in the form

$$I(\theta) = |\psi|^2 = 4|c_n|^2\sin^2(n\theta) + |c_0|^2 = 2|c_n|^2 - 2|c_n|^2\cos(2n\theta) + |c_0|^2 \ , \qquad \text{(A9)}$$

where we again omit the radial dependence. In the approximation that the azimuthal and radial degrees of freedom of the image are factored, the image can be decomposed in terms of azimuthal Fourier components in the form

$$I(\theta) = \sum_\ell \ I_\ell \exp(i\,\ell\theta) \ . \qquad \text{(A10)}$$

These coefficients can be measured experimentally and compared with predictions of the sorter-based OAM decomposition.

Azimuthal Fourier decomposition of the image therefore only has components I_ℓ with ℓ=±2n and 0. By using Eqs A9 and A10, we find that

$$I_0 = 2|c_n|^2 + |c_0|^2 \qquad \text{(A11a)}$$

$$I_{2n} = |c_n|^2 \qquad \text{(A11b)}$$

A more realistic description of the hologram should include absorption and therefore an amplitude modulation superimposed onto the phase with the same frequency. Although the formulae are given in Ref. 27, it is sufficient to write δ → δ+ia, where a<< δ . In the same way, Eq. A8 can be rewritten with real coefficients $c_{1r,}c_{1i}, c_{0r}, c_{0i}$ in the form

$$\psi = 2(c_{1r} + ic_{1i})\sin(n\theta) + \mathrm{i}(c_{0r} + ic_{0i}) \ ,$$

where $c_{1i} \ll c_{1r}$ and $c_{1i} \ll c_{1r}$. After a few simple steps, we find that the main contribution of the additional terms is

$$I_n = -4c_{0i}c_{1r} + 4c_{0r}c_{1i} \ . \qquad \text{(A12)}$$

We therefore expect an additional Fourier component that is related to the superimposed and unwated amplitude modulation effect of the hologram. The contribution from such components is very small.

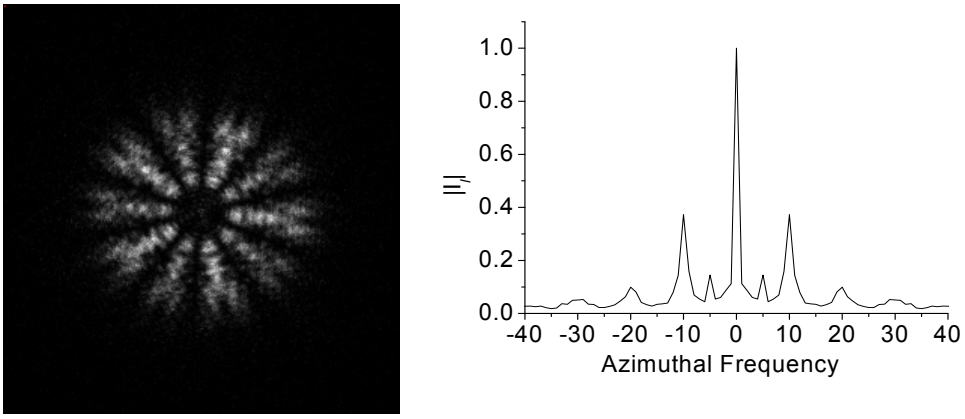

Fig A4 : (a) Experimental defocused image of a petal beam corresponding to the left image in Fig. A3 for $\ell = \pm 5$ *. (b) OAM coefficients of this image obtained by its digital analysis.*

An experimental defocused image of a petal beam generated by the hologram shown on the left of Fig, A3 is shown in Fig. A4. alongside a digitally-calculated azimuthal Fourier decomposition of the same image. The procedure for extracting the I_ℓ coefficients follows previous work (Ref. A1) and is based on a digital version of the OAM sorter, where the intensity is mapped to polar coordinates and Fourier transformed. The results indicate that the dominant azimuthal Fourier coefficients I_ℓ correspond to values of $\ell = \pm 10$ and 0, which is consistent with the assumption that meaningful values of c_ℓ correspond to $\ell = \pm 5$. There is also a slight absorption effect, which introduces an image term I_ℓ at $\ell = \pm 5$.

By using Eq. A11, we find $|c_0|^2 = I_0 - 2I_{2n}$ and that a contribution c_0 is present with an intensity ratio $\frac{|c_0|^2}{|c_1|^2} \approx 50\%$ that is approximately consistent with the spectrum shown in Fig. 3 of the main text.

A4: Analytical model for phase mismatch

The experimental OAM spectrum from a uniform beam is not a single *sinc* peak, but contains additional oscillations and broadening, We show here that these deformations arise primarily from a size mismatch, which can be estimated from Eq. 2 and expressed in a real coordinate formalism using Eq. A3 or otherwise by

[1] V. Grillo, G. C. Gazzadi, E. Mafakheri, S. Frabboni, E. Karimi, and R. W. Boyd, *Holographic Generation of Highly Twisted Electron Beams*, Phys. Rev. Lett. **114**, 034801 (2015).

$$\varphi = \frac{Ls}{\lambda}\cos(Kx')\exp(-Ky'), \qquad \text{(A13)}$$

where $K = \frac{1}{sf}$.

The beam can be approximated as a line (as shown in Fig. A5 and Ref. [27]) at a given value of $y' = sf\ln\left(\frac{R}{L}\right)$, which corresponds to the outer rim of the beam in the S1 plane at radius $R = \sqrt{x^2 + y^2}$.

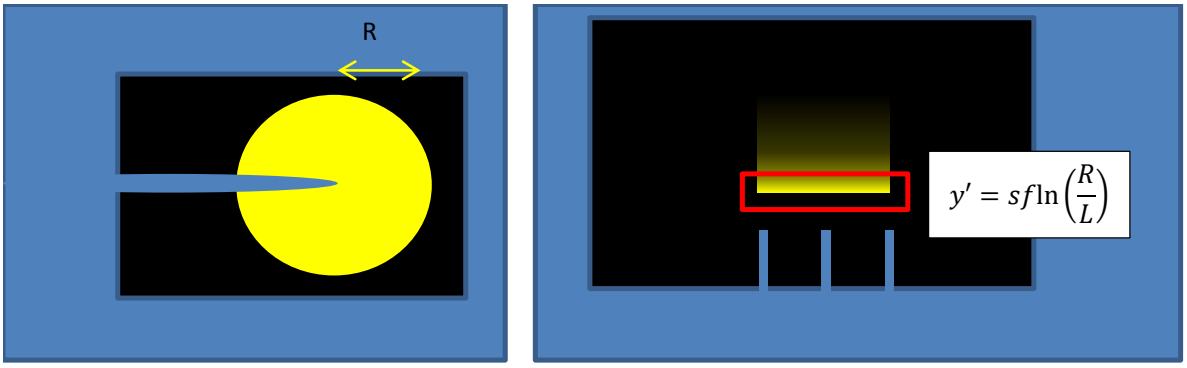

Fig A5 Schematic illustration of a uniform beam approaching sorter 1 and sorter 2 .

The unmatched phase that results from the mismatch $m = \Delta K/K$ between element S2 and the size of the diffracted beam is

$$\Delta\varphi = \frac{s\mathrm{R}}{\lambda}\left[\cos\left(\frac{x\prime}{sf}\right) - \cos\left(\frac{x\prime}{sf}(1+\mathrm{m})\right)\right] \approx \frac{s\mathrm{R}}{\lambda}\mathrm{m}\left(\frac{x'}{sf}\right)^2 - \frac{s\mathrm{R}}{\lambda}\frac{1}{6}\mathrm{m}\left(\frac{x\prime}{sf}\right)^4, \qquad \text{(A14)}$$

where Taylor series in *m* and *x'* have been truncated at 4th order. The quadratic term can be difficult to notice in experiments, since the microscope operator adjusts parameters such as defocus, which can compensate for it. The leading uncompensated term produces a maximum phase shift of $\Delta\varphi_{max} \approx 16\, sR\, m/\lambda$. For $sR/\lambda = 1$ and a value for *m* of 4%, the phase profile has the shape shown in Fig. A6.

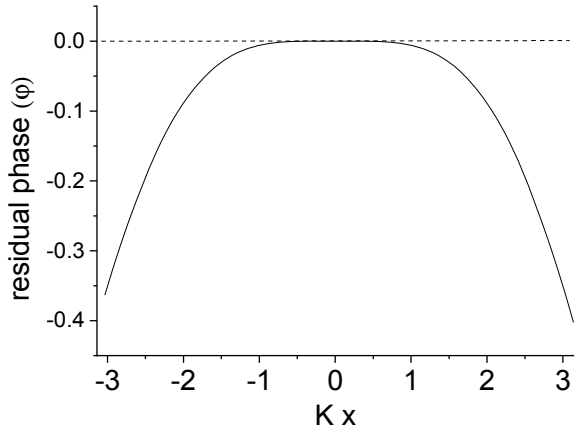

Fig A6 Residual phase when sorter 2 does not perfectly compensate the phase of diffraction of sorter 1.

A "flat" phase region is obtained over approximately half of the angular range. Changing the value of *m* does not change the shape of the curve, but only the phase scaling factor. One can conclude that: 1) The central "flat" region is responsible for the main OAM peak, whereas the phase tails are responsible for the OAM spectrum background; 2) In most cases, the flat region extends over only approximately half of the *x'* range, which accounts for the fact that $\Delta\ell \approx 2$ is observed in most cases; 3) It is possible to improve the OAM resolution by reducing *s, i.e.*, the voltage applied to element S1, or *R*, the size of the beam at the entrance of the sorter.

A5. Lens + sorter simulation

We implemented a numerical method to simulate the OAM spectroscopy experiment based on a full wave calculation and free space propagation, in order to quantitatively describe the effects of several aberrations and misalignments on the final resolution. The beam is free-space propagated between the elements using the Fresnel-Kirchhoff integral

$$U_z(u,v) = \frac{e^{ikz}}{i\lambda z}\iint U_0(x,y)\, e^{-ik\frac{xu+yv}{z}} dxdy \ .$$

The lens is defined by a quadratic phase element

$$T = exp\left(\frac{i(x^2+y^2)}{2f\lambda}\right) .$$

The sorters are defined by the phase distributions reported in the text. Calculations were performed numerically on an 8k x 8k pixel matrix using a Fourier transform algorithm for convolutions. The code was written in Matlab and C.

Even for the largest allowed sampling, the phase gradient was limited by the number of pixels. In order to correctly compute the lens effect, the phase should not vary too rapidly. The phase difference between adjacent pixels should typically be less then π, such that

$$\frac{d\,\phi}{d\,n} < \pi \ .$$

Based on this criterion, the minimum usable focal distance is

$$f_{min} = \frac{2L^2}{\lambda n} \approx 198\,mm \ .$$

We are therefore limited to relatively large focal distances, making it impossible to numerically simulate the objective lens (*i.e.*, a thick and strong lens).

Fortunately, the curvature of the diverging beam from the sample and the focusing effect are nearly compensated at the entrance of the sorter in the objective back focal aperture. We can therefore simulate an equivalent configuration, in which the sorter 1 element is illuminated by a weakly convergent beam.

A second lens is finally placed after sorter 2. The simulated optical configuration is shown in Fig. A7

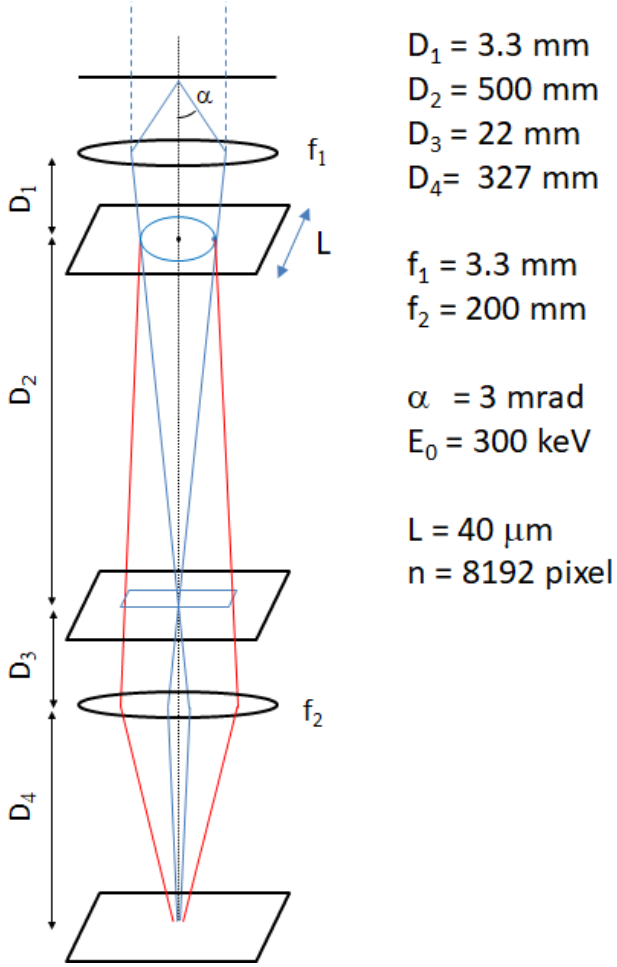

Fig A7 Schematic illustration of the sorting apparatus, including two main lenses.

We used this approach to analyze the effect of different parameters on OAM spectrum resolution. The more detrimental parameters, which should therefore be addressed with care, include misalignment between the two sorter elements, their relative rotation, the size mismatch and the defocus of the lenses. With the exception of size mismatch and relative rotation, these factors can be adjusted easily in real time during operation.